

Anomalous Hall viscosity of altermagnets

Iksu Jang,¹ Rui Aquino,^{2,3,4} Jörg Schmalian,^{1,5} and Rafael M. Fernandes^{2,3}

¹*Institute for Theory of Condensed Matter, Karlsruhe Institute of Technology, Karlsruhe 76131, Germany*

²*Department of Physics, The Grainger College of Engineering,*

University of Illinois Urbana-Champaign, Urbana, Illinois 61801, USA

³*Anthony J. Leggett Institute for Condensed Matter Theory, The Grainger College of Engineering,*
University of Illinois Urbana-Champaign, Urbana, Illinois 61801, USA

⁴*ICTP South American Institute for Fundamental Research, São Paulo, SP, Brazil*

⁵*Institute for Quantum Materials and Technologies, Karlsruhe Institute of Technology, Karlsruhe 76131, Germany*

(Dated: June 26, 2026)

We show that the phonon Hall viscosity at zero magnetic field is a natural probe of altermagnetism. First, we demonstrate that the finite elements of the Hall viscosity tensor unambiguously distinguish altermagnets from ferromagnets and conventional antiferromagnets. We then microscopically compute the Hall viscosity in models for d -wave and g -wave altermagnets, and find a strong sensitivity to electronic spectrum features such as gapped Dirac points and Lifshitz transitions. This sensitivity reflects a strain-space Berry curvature monopole, which contrast to the multipolar character of the standard momentum-space Berry curvature in altermagnets. Since the Hall viscosity can be probed experimentally through magneto-acoustic measurements, it provides a compelling method to probe the broken symmetries and topology of insulating altermagnets.

Altermagnets are compensated magnets that are invariant under a combination of time reversal and a crystalline operation that involves rotations, such as proper rotations, mirror reflections, glide reflections, and screw rotations [1, 2]. This symmetry endows altermagnets with distinctive d -wave, g -wave, or i -wave characters, manifested both in the momentum dependence of the spin-splitting of the electronic bands and in the real-space spin density [3, 4]. However, the experimental challenges in directly probing momentum-space spin-splitting motivates the search for global response functions that not only encode the symmetry of altermagnets, but also their unique topological properties [5–11].

The anomalous Hall conductivity, a primary probe of non-trivial topology [12, 13], vanishes in pure altermagnets due to the multipolar character of their momentum-space Berry curvature [11]. In the presence of spin-orbit coupling (SOC), it can become non-zero either for specific moment directions [14–18] or when external uniaxial strain is applied [11]. Nevertheless, most altermagnetic candidates are insulators [2, 19–21], which limits the use of the Hall conductivity as a probe of altermagnetism. Lattice responses, on the other hand, can be measured in both metals and insulators. It is thus valuable to elucidate the lattice responses of altermagnets, particularly given their unique magneto-elastic properties, of which piezomagnetism is the posterchild [22–37].

Here, we show that the Hall viscosity, which is measured through sound waves rather than static strain, provides a natural probe of altermagnetic order and of the underlying topology of the band structure. Also known as phonon Hall viscosity, it is the antisymmetric, non-dissipative part of the viscosity tensor that relates time-dependent strain to transverse stress (Fig. 1). While previous works focused on the Hall viscosity of magnetic insulators and quantum Hall systems in an external magnetic field [38–48], our focus is on the zero-field (i.e., anomalous) response. In contrast to antiferromagnets, which cannot have an anomalous Hall

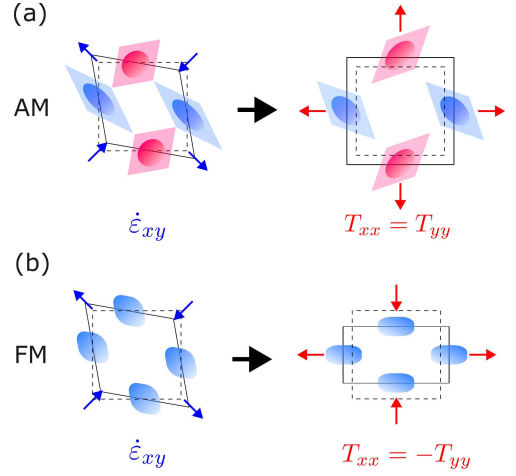


FIG. 1. Non-dissipative stress components T_{xx} and T_{yy} generated by a dynamic shear strain $\dot{\epsilon}_{xy}$ due to the anomalous Hall viscosity in a tetragonal system. Red and blue refer to spin-up and spin-down densities. The stress symmetry is determined by the type of magnetic state: in a d -wave altermagnetic (AM) state, a symmetry-preserving static stress $T_{xx} = T_{yy}$ is generated (a), while in a ferromagnetic (FM) state, tetragonal-symmetry-breaking stress $T_{xx} = -T_{yy}$ appears (b).

viscosity, we find that ferromagnets and altermagnets display finite but distinct Hall viscosity tensor elements at zero field. To elucidate the microscopic mechanism, we calculate the anomalous Hall viscosity in representative minimal models for tetragonal d -wave and hexagonal g -wave altermagnetism. In both cases, the Hall viscosity reflects a net strain-space Berry curvature monopole, in sharp contrast to the multipolar character of the momentum-space Berry curvature that governs the anomalous Hall conductivity.

This connection with the strain-space Berry curvature makes the Hall viscosity highly sensitivity to special features of the altermagnetic electronic states. In d -wave altermagnets, we find it to be dominated by the spin-polarized Dirac points

that are gapped by the SOC [6]. This allows us to interpret the Hall viscosity as the ‘‘Hall conductivity’’ due to emergent spin-dependent electromagnetic gauge fields generated by dynamic strain. In g -wave altermagnets, we show that the strain-induced modification of the SOC is the main feature responsible for a finite anomalous Hall viscosity, which is strongly impacted by the saddle-points of the electronic bands. Importantly, while SOC is essential for a non-zero Hall viscosity, weak SOC does not necessarily imply a small Hall viscosity. In fact, the magnitude of our calculated Hall viscosity is comparable to what was recently reported for α -RuCl₃ using the acoustic Faraday effect [49].

Symmetry analysis: At low frequencies, dynamical stresses $T_{ij}(t)$ in a many-body system are related to time-dependent strain $\varepsilon_{kl}(t)$ via

$$T_{ij}(t) = C_{ijkl}\varepsilon_{kl}(t) + \eta_{ijkl}\partial_t\varepsilon_{kl}(t). \quad (1)$$

The first term is the elastic tensor, whereas the second term usually accounts for the fact that deformations performed at a finite rate are dissipative and generate heat. However, the elements η_{ijkl}^H of the viscosity tensor η_{ijkl} that are antisymmetric under $ij \longleftrightarrow kl$ are non-dissipative. This Hall viscosity tensor is odd under time reversal and even under inversion, giving rise to the effective elastic action

$$S_{\text{eff}} = \frac{1}{2} \int_{x,t} \eta_{ijkl}^H \varepsilon_{ij} \partial_t \varepsilon_{kl}, \quad (2)$$

with $\int_{x,t}$ denoting integration over space and time. This elastic (phonon) Hall viscosity should not be confused with the viscoelastic Hall response of an electronic fluid in the hydrodynamic regime [40, 50–52]. Since a finite Hall viscosity requires broken time-reversal symmetry (TRS), it has often been investigated as a response to an external magnetic field [43, 45–47]. For instance, in a 2D isotropic system subjected to a magnetic field, the only allowed non-zero element is $\eta_{xxxy}^H = -\eta_{yyxy}^H$, corresponding to the stress-strain relationship shown in Fig. 1(b). By symmetry, a ferromagnet must display the same non-zero element, but at zero applied field, corresponding to an anomalous Hall viscosity. However, there are other ordered phases that break TRS, such as antiferromagnetic and altermagnetic orders. While the combination of time-reversal and translational (or inversion) symmetries enforce $\eta_{ijkl}^H = 0$ in antiferromagnets, the symmetries of altermagnetism are generally compatible with finite Hall viscosity tensor elements at zero fields.

To show this, we employ group theory to decompose the 15-dimensional reducible representation consisting of the non-zero elements of η_{ijkl}^H into irreducible representations (irreps) of the point group describing the paramagnetic phase. This task is greatly simplified by expressing η_{ijkl}^H in terms of the so-called Jahn symbols [53] as $a \{ [V^2] [V^2] \}$ [54]. For example, in a tetragonal system with point group D_{4h} , we find:

$$a \{ [V^2] [V^2] \} \rightarrow A_{1g}^- \oplus 2A_{2g}^- \oplus 2B_{1g}^- \oplus 2B_{2g}^- \oplus 4E_g^-, \quad (3)$$

where the minus superscript denotes a TRS-odd irrep. These irreps correspond to different even-parity $\mathbf{Q} = 0$ magnetic orders in the presence of SOC [25]. A_{2g}^- and E_g^- transform like the out-of-plane and in-plane magnetization, respectively, thus describing either ferromagnetic or mixed altermagnetic order parameters (i.e., altermagnets with weak ferromagnetism due to SOC). In contrast, A_{1g}^- , B_{1g}^- , and B_{2g}^- describe pure altermagnetic order parameters (i.e., with a symmetry-enforced zero magnetization) with, respectively, g -wave, d_{xy} -wave, and $d_{x^2-y^2}$ -wave spin-splitting symmetry. Thus, Eq. (3) implies that each type of magnetic order parameter is associated with a unique combination of non-zero anomalous Hall viscosity tensor elements, demonstrating the suitability of η_{ijkl}^H to distinguish between magnetic orders. Consider, for instance, the cases of a $d_{x^2-y^2}$ altermagnet (B_{2g}^-) and a ferromagnet with out-of-plane magnetization (A_{2g}^-). While the same anomalous Hall viscosity elements are non-zero in both cases, they have different relative signs: $\eta_{xxxy}^H = \eta_{yyxy}^H \neq 0$ for the altermagnet and $\eta_{xxxy}^H = -\eta_{yyxy}^H \neq 0$ for the ferromagnet, resulting in different stresses generated by the same dynamic shear strain, see Fig. 1. The End Matter shows the symmetry-allowed η_{ijkl}^H for altermagnets in various point groups.

Microscopic expression: To investigate the microscopic origin of the anomalous Hall viscosity in altermagnets, we consider a system described by Bloch states $|u_{k,b}\rangle$ with crystal momentum \mathbf{k} and band index b . The full Hamiltonian is $\mathcal{H}_{\mathbf{k}} = \mathcal{H}_{\mathbf{k},0} + \mathcal{H}_{\mathbf{k},\varepsilon}$ with a strain-free contribution $\mathcal{H}_{\mathbf{k},0} = \sum_b \xi_{k,b} |u_{k,b}\rangle \langle u_{k,b}|$ and a strain-dependent term $\mathcal{H}_{\mathbf{k},\varepsilon} = \varepsilon_{ij} \sum_{bb'} \gamma_{bb'}^{ij}(\mathbf{k}) |u_{k,b}\rangle \langle u_{k,b'}|$. The coupling matrices $\gamma_{bb'}^{ij}$ determine the electron-phonon coupling to acoustic lattice vibrations in the band basis [11]. The stress tensor T_{ij} generated by a dynamic strain that slowly varies in time can then be obtained through the quasi-adiabatic expansion [38]:

$$T_{ij} = \left\langle \frac{\delta \mathcal{H}_{\mathbf{k}}}{\delta \varepsilon_{ij}} \right\rangle = \frac{\delta \langle \mathcal{H}_{\mathbf{k}} \rangle}{\delta \varepsilon_{ij}} + \sum_{kl,b} \Omega_{ijkl}^{(b)}(\mathbf{k}) \partial_t \varepsilon_{kl}, \quad (4)$$

from which we readily identify the Hall viscosity

$$\eta_{ijkl}^H = \frac{\hbar}{V} \sum_{\mathbf{k},b} f(\xi_{k,b}) \Omega_{ijkl}^{(b)}(\mathbf{k}), \quad (5)$$

and the strain-space Berry curvature

$$\begin{aligned} \Omega_{ijkl}^{(b)}(\mathbf{k}) &= i \left(\langle \partial_{\varepsilon_{ij}} u_{k,b} | \partial_{\varepsilon_{kl}} u_{k,b} \rangle - \langle \partial_{\varepsilon_{kl}} u_{k,b} | \partial_{\varepsilon_{ij}} u_{k,b} \rangle \right) \\ &= 2\text{Im} \sum_{b' \neq b} \frac{\gamma_{b'b}^{ij}(\mathbf{k})^* \gamma_{b'b}^{kl}(\mathbf{k})}{(\xi_{kb} - \xi_{kb'})^2}, \end{aligned} \quad (6)$$

where V is the volume and f is the Fermi-Dirac distribution. In Ref. [55], we derive this result without invoking the quasi-adiabatic approximation. In order for the Hall viscosity in Eq. (6) to be finite, $\mathcal{H}_{\mathbf{k},\varepsilon}$ must not commute with $\mathcal{H}_{\mathbf{k},0}$, otherwise $\gamma_{b'b}^{ij}$ is diagonal. Moreover, SOC must be present to induce local Berry curvature. To elucidate the microscopic properties that govern $\Omega_{ijkl}^{(b)}$, we compute it in minimal models for tetragonal d -wave and hexagonal g -wave altermagnets.

Tetragonal d -wave altermagnets: The Lieb lattice model of Ref. [6] (see also [7, 56]) provides a convenient description of a d -wave altermagnet on the tetragonal lattice (irrep B_{2g}^-), being realized in materials of the families $R_2Mn_2Se_2O_3$ [57–59], AV_2Te_2O [22, 60–62] and Fe_2X_2O ($X=Cl, Br, I$) [63]. The model shown in Fig. 2 (a) has non-magnetic atoms on the sites of a square lattice and magnetic atoms on the bond centers with opposite out-of-plane spins related by a 90° crystal rotation. The strain-free Hamiltonian is thus invariant under a combination of a 90° rotation and time-reversal [6, 7]

$$\mathcal{H}_{k,0} = \varepsilon_{0,k} + t_{1,k}\tau_1 + t_{3,k}\tau_3 + \vec{\lambda}_k \cdot \vec{\sigma} \tau_2 + J\phi\tau_3\sigma_3, \quad (7)$$

with sublattice and spin-space Pauli matrices τ_i and σ_i , respectively. The first three terms depend on the hopping parameters shown in Fig. 2 (a) through $\varepsilon_{0,k} = -t_2 f_{0,k}$, $t_{1,k} = -t_1 f_{1,k}$, and $t_{3,k} = -t_d f_{3,k}$, with $t_2 = (t_{2a} + t_{2b})/2$ and $t_d = (t_{2a} - t_{2b})/2$, and lattice harmonics $f_{1,k} = 4 \cos \frac{k_x}{2} \cos \frac{k_y}{2}$ and $f_{0(3),k} = 2(\cos k_x \pm \cos k_y)$. The SOC term has the simple form $\vec{\lambda}_k = \lambda \sin \frac{k_x}{2} \sin \frac{k_y}{2} \hat{z}$ and ϕ is the altermagnetic order parameter. The symmetry-allowed strain Hamiltonian contains the three distinct in-plane strain irreps of the tetragonal group (see also [11, 64])

$$\mathcal{H}_{k,\varepsilon} = (\varepsilon_{xx} + \varepsilon_{yy})\gamma_k^{(A_{1g})} + (\varepsilon_{xx} - \varepsilon_{yy})\gamma_k^{(B_{1g})} + 2\varepsilon_{xy}\gamma_k^{(B_{2g})} \quad (8)$$

with coupling matrices:

$$\begin{aligned} \gamma_k^{(A_{1g})} &= g_0^{(A_{1g})} f_{0,k}\tau_0 + g_1^{(A_{1g})} f_{1,k}\tau_1 + g_3^{(A_{1g})} f_{3,k}\tau_3, \\ \gamma_k^{(B_{1g})} &= 2g^{(B_{1g})}\tau_3, \\ \gamma_k^{(B_{2g})} &= -2g^{(B_{2g})} \sin \frac{k_x}{2} \sin \frac{k_y}{2} \tau_1. \end{aligned} \quad (9)$$

Here, $g_i^{(\Gamma)}$ are coupling constants with magnitudes comparable to the hopping parameters [11]. The electronic dispersion of $\mathcal{H}_{k,0}$ has four spin-polarized Dirac points at the Brillouin zone boundaries for $|\phi| < \phi_c = |4t_d/J|$, which are gapped by SOC, as shown by the green lines at momenta at $\mathbf{k}_{*,1}$ and $\mathbf{k}_{*,2}$ in Fig. 2 (b). Being sources of large Berry curvature, these gapped Dirac points determine not only the behavior of the momentum-space Berry curvature quadrupole [6, 11, 35, 65], but also the properties of the strain-space Berry curvature of Eq. (5). The latter, in turn, gives the non-zero Hall viscosity tensor elements in the altermagnetic phase, which according to our group theory analysis are $\eta_{xxxy}^H = \eta_{yyxy}^H \neq 0$.

Figs. 2 (c)-(d) show $\frac{1}{2}(\Omega_{xxxy}^{(2)} \pm \Omega_{yyxy}^{(2)})$, respectively, computed at the second band in Fig. 2 (b). Both show large local Berry curvature values near the gapped Dirac points at $\mathbf{k}_{*,1}$ and $\mathbf{k}_{*,2}$. While for $\Omega_{xxxy}^{(2)} + \Omega_{yyxy}^{(2)}$ these values have the same sign near all Dirac points, resulting in a Berry curvature monopole, for $\Omega_{xxxy}^{(2)} - \Omega_{yyxy}^{(2)}$ the Berry curvature changes sign under a 90° rotation, resulting in a Berry curvature quadrupole consistent with the quadrupolar structure of the momentum-space Berry curvature $\tilde{\Omega}_{xy}$ [11]. Thus, the strain-space Berry

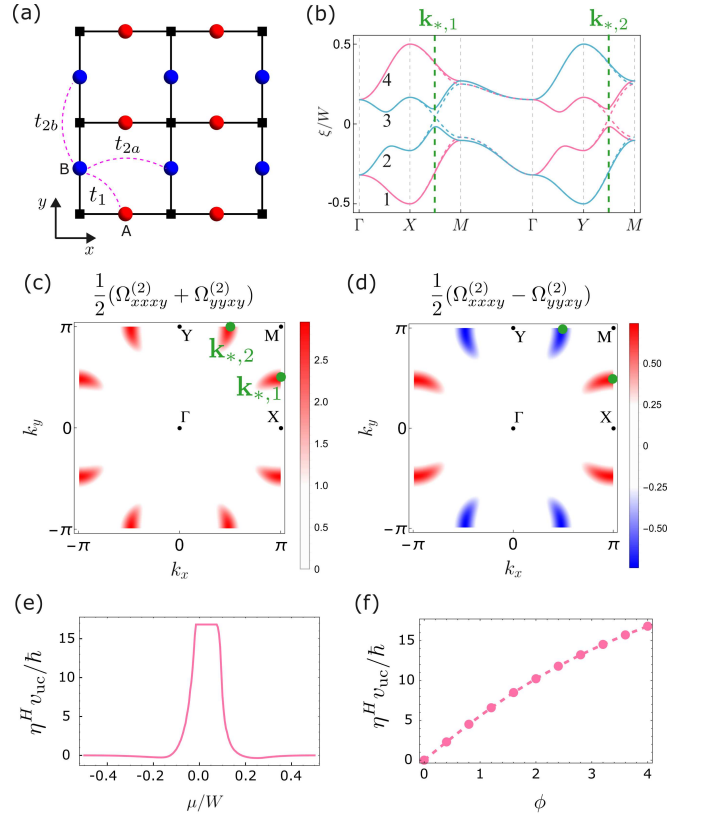


FIG. 2. (a) Lieb-lattice model for d -wave altermagnetism [6] and (b) the corresponding band structure with bands labeled by (1,2,3,4). Pink and blue refer to spin up and down states, respectively. The solid (dashed) lines correspond to non-zero (zero) SOC. The Dirac points are located along the green dashed lines. (c) Strain-space Berry curvature elements of the second band, (c) $\frac{1}{2}(\Omega_{xxxy}^{(2)} + \Omega_{yyxy}^{(2)})$ and (d) $\frac{1}{2}(\Omega_{xxxy}^{(2)} - \Omega_{yyxy}^{(2)})$. (e) Hall viscosity $\eta^H \equiv \frac{1}{2}(\eta_{xxxy}^H + \eta_{yyxy}^H) = \eta_{xxxy}^H = \eta_{yyxy}^H$ as a function of the chemical potential and (f) of the altermagnetic order parameter ϕ at $\mu = 0$. Here, v_{uc} is the unit cell volume. The values of the tight binding parameters used here are shown in the SM [55].

curvature can be uniquely employed to disentangle the intrinsic multipolar structure of the Berry curvature of altermagnets. Using Eq. (5), these results give $\eta_{xxxy}^H = \eta_{yyxy}^H \neq 0$, in agreement with our group-theory analysis. Moreover, as shown in Fig. 2 (e) and (f), not only is η^H proportional to the altermagnetic order parameter ϕ , but it also is the largest for the chemical potential values for which the system is in the insulating phase. This demonstrates the suitability of exploiting the Hall viscosity to measure altermagnetic order in insulators.

To gain further insights into the topological origin of the Hall viscosity, we expand the Hamiltonian around the Dirac points labeled by valley $\kappa = \pm 1$ and spin $\sigma = \uparrow, \downarrow$, as shown in Fig. 3(a). Inclusion of SOC leads to the characteristic Dirac Hamiltonian (see [55]):

$$\mathcal{H} = \sum_{\sigma, \kappa, i=x,y} \{v_i^{\sigma, \kappa} (p_i - \mathcal{A}_i^{\sigma, \kappa}) \alpha_i^\sigma + m^\sigma \beta\} \quad (10)$$

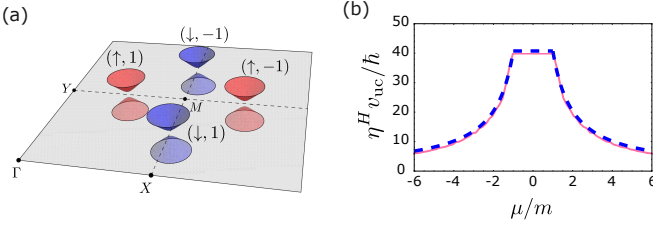


FIG. 3. (a) The four spin-polarized Dirac points of the Lieb lattice model are located at the Brillouin zone boundaries when $|\phi| < \phi_c$. They are labeled by their spin ($\sigma = \uparrow, \downarrow$) and valley ($\kappa = \pm 1$) quantum numbers (σ, κ). (b) Comparison between the Hall viscosity $\eta^H = \eta_{xxxy}^H = \eta_{yyxy}^H$ from the full tight-binding model (pink solid line) and from the Dirac theory of Eq. (12) (blue dashed line). For the parameters values used here, see the SM [55].

with Dirac matrices α_i^σ and β , velocities $v_i^{\sigma, \kappa}$, and SOC-generated mass $m^\sigma = \sigma \lambda \sqrt{1 - \phi/\phi_c}$. Crucially, strain appears as an electromagnetic gauge field with

$$\begin{aligned} \varepsilon_{xx} \pm \varepsilon_{yy} &\propto \mathcal{A}_x^{\uparrow, \kappa} \mp \mathcal{A}_y^{\downarrow, \kappa}, \\ \varepsilon_{xy} &\propto \mathcal{A}_y^{\uparrow, \kappa} + \mathcal{A}_x^{\downarrow, \kappa}. \end{aligned} \quad (11)$$

This is analogous to the emergent magnetic fields in graphene arising from static but spatially varying strain [66, 67]. In our case, because the strain is dynamic and the system is in the altermagnetic phase, the gauge fields correspond to emergent electrical fields, like in Refs. [68–71], which are however spin-dependent. As a result, the Hall viscosity can be expressed in terms of the Hall conductivity σ_{xy}^H (of unit charge $e = 1$) of a single Dirac point as:

$$\eta_{xxxy}^H = \eta_{yyxy}^H = C_0 \sigma_{xy}^H = \frac{C_0}{\hbar} \begin{cases} \frac{\text{sign}(m)}{4\pi} & \text{if } \mu_r^2 < m^2 \\ \frac{m}{4\pi|\mu_r|} & \text{if } \mu_r^2 > m^2 \end{cases}, \quad (12)$$

where μ_r is the chemical potential relative to the Dirac point, $m = \lambda \sqrt{1 - \phi/\phi_c}$ and $C_0 = 8\hbar^2 g^{(B_{2g})} g_3^{(A_{1g})} / (v_{uc} t_1 t_d)$. As shown in Fig. 3(b), this expression is in quantitative agreement with the full tight-binding calculation of the Hall viscosity, at least for small SOC-induced gap [72]. We emphasize that Eq. (12) does not imply that the system has an anomalous Hall conductivity; instead, it simply expresses the fact that the anomalous Hall viscosity is proportional to the anomalous Hall conductivity of a single Dirac point, generated by the emergent gauge fields of Eq. (11). Once the contributions of all Dirac points are added, only the anomalous Hall viscosity survives.

It is also instructive to express Eq. (2) in terms of the emergent gauge fields:

$$S_{\text{eff}} = \sigma_{xy}^H \sum_{\sigma, \kappa} \sigma \int_{x,t} \varepsilon_{ij} \mathcal{A}_i^{\sigma, \kappa} \partial_t \mathcal{A}_j^{\sigma, \kappa}, \quad (13)$$

with ε_{ij} the 2D Levi-Civita symbol. This action is noting but the temporal version of two Chern-Simons actions with opposite Hall conductivities for the two spin sectors, ensuring a vanishing Hall conductivity but a finite Hall viscosity.

Hexagonal g-wave altermagnets: The tetragonal d -wave altermagnet studied above is essentially a 2D model. In contrast, g -wave altermagnetism in hexagonal lattices, as realized in CrSb [73–76], MnTe [77–81], and $\text{Co}_{1/4}\text{NbSe}_2$ [82–85], is intrinsically 3D. To investigate their Hall viscosity, we adopt the minimal model of Ref. [7], with point group D_{6h} . As illustrated in Fig. 4 (a), the two magnetic atoms are not on the same plane, but are related by a sixfold screw rotation, i.e., a sixfold rotation followed by a half-translation along the z -axis. The Hamiltonian $\mathcal{H}_{\mathbf{k}, 0}$ has the same form of Eq. (7), but the functions depend explicitly on k_z and the SOC term $\vec{\lambda}_{\mathbf{k}}$ has in-plane components (see the Supplementary Material [55]).

We focus on moments aligned along the z -axis, relevant for CrSb and $\text{Co}_{1/4}\text{NbSe}_2$, in which case the altermagnetic order parameter ϕ in Eq. (7) transforms as the B_{1g}^- irrep of D_{6h} . This gives spin-split nodal planes along $k_z = 0$ and $k_y = 0$ (and symmetry-related planes), which are partially gapped by SOC, as shown in the electronic dispersion of Fig. 4 (b). In this case, our group-theory analysis predicts non-zero Hall viscosity tensor components $\eta_{xxxz}^H = -\eta_{yyxz}^H = -\eta_{xyyz}^H$. We therefore consider the coupling matrices $\gamma_{b'b}^{ij}$ in $\mathcal{H}_{\mathbf{k}, \varepsilon}$ associated with the in-plane and out-of-plane shear strains, $(\varepsilon_{xx} - \varepsilon_{yy}, \varepsilon_{xy})$ and $(\varepsilon_{xz}, \varepsilon_{yz})$.

Fig. 4 (c) displays our results for $\frac{1}{2}(\Omega_{xxxz}^{(4)} - \Omega_{yyxz}^{(4)})$ along the $k_z = 0$ plane, regularized for clearer presentation (see SM) and calculated at the band 4 highlighted in Fig. 4 (b). This Berry curvature component is even with respect to reflections along the k_x and k_y mirrors, and thus averages to a finite value. Fig. 4 (d) shows the behavior of the in-plane integrated Berry curvature as a function of k_z , $\frac{1}{2}(\bar{\Omega}_{xxxz}^{(4)} - \bar{\Omega}_{yyxz}^{(4)})$ where $\bar{\Omega}_{xx(yy)yz}^{(4)}(k_z) = \int_{k_x, k_y} \Omega_{xx(yy)yz}^{(4)}(\mathbf{k})$. Its sudden change around $\frac{k_z}{2\pi} \approx 0.25$ originates from a Lifshitz transition of the Fermi surface, which in turn is manifested as sudden changes of the Hall viscosity $\eta_{xxxz}^H = -\eta_{yyxz}^H$ as a function of the chemical potential μ in Fig. 4(e), thus showcasing the sensitivity of the Hall viscosity to the topology of the band structure (a detailed analysis is shown in [55]). Importantly, a non-zero η^H requires the strain Hamiltonian to also modify the SOC. Without such a strain-induced SOC term, we find a vanishing Hall viscosity. Finally, Fig. 4(f) directly demonstrates the proportionality between the anomalous Hall viscosity and the altermagnetic order parameter ϕ .

Discussion : The calculated Hall viscosity η^H in Fig. 2(e) and Fig. 4(e) acquires values of the order of $10\hbar/v_{uc}$ which, taking a typical unit cell volume $v_{uc} = a_0^3$ with $a_0 = 5\text{\AA}$, gives $\eta^H \sim 8.15 \mu\text{Pa}\cdot\text{s}$. These are comparable to the values recently reported in α -RuCl₃ under an external magnetic field [49], measured through the acoustic Faraday effect [49, 86–89]. In a hexagonal system like α -RuCl₃, this effect arises because the Hall viscosity term $\eta_{xxxy}^H = -\eta_{yyxy}^H$ generated by the magnetic field lifts the degeneracy of the transverse acoustic waves propagating along the c -axis, which results in a rotation of the circular polarization of an incident transverse strain wave. In a hexagonal g -wave altermagnet like CrSb, however, the

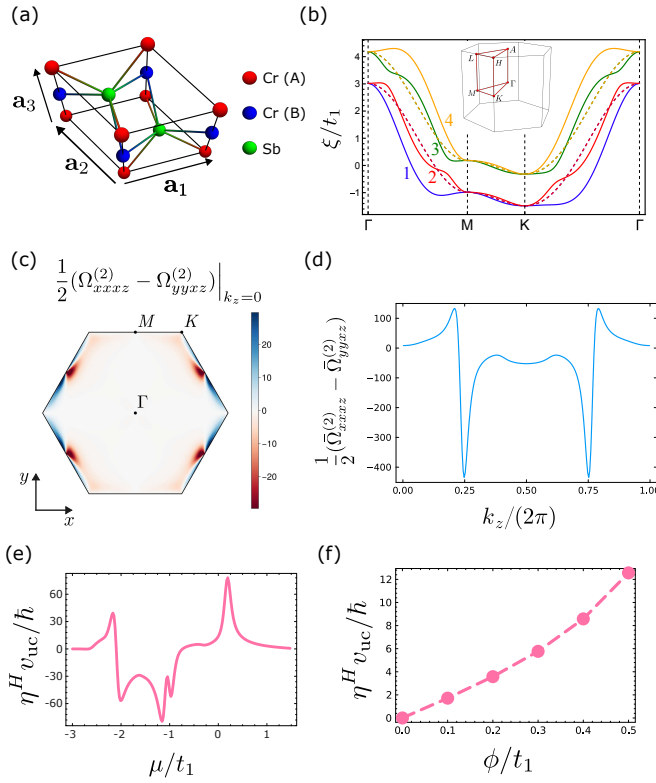


FIG. 4. (a) Hexagonal lattice model for g -wave altermagnetism. Open and closed symbols refer to atoms away and at the $z = 0$ plane, respectively. (b) Band structure of the model with band labels (1,2,3,4); the inset shows the first Brillouin zone. Solid and dashed lines represent the cases with and without SOC, respectively; note that, without SOC, there is no spin-splitting at $k_z = 0$. The values of the parameters used here are given in the SM [55]. (c) Berry curvature component $(\Omega_{xxxz}^{(4)} - \Omega_{yyxz}^{(4)})/2$. (d) k_z -dependence of the Berry curvature $(\bar{\Omega}_{xxxz}^{(4)} - \bar{\Omega}_{yyxz}^{(4)})/2$ integrated over the in-plane momenta. (e) Hall viscosity $\eta^H = \eta_{xxxz}^H = -\eta_{yyxz}^H$ as a function of the chemical potential μ and (f) of the altermagnetic order parameter ϕ for fixed $\mu/t_1 = 0.5$.

zero-field Hall viscosity term $\eta_{xxxz}^H = -\eta_{yyxz}^H$ does not mix the c -axis sound waves. Nevertheless, one can still exploit the near-degeneracy of the transverse modes propagating along a direction that is tilted slightly away from the c -axis. Because sound propagation is birefringent along this direction, the linear polarization of an incident transverse wave will generally rotate even in the paramagnetic phase. However, the combination of near-degenerate sound velocities with the form factor of $\eta_{xxxz}^H = -\eta_{yyxz}^H$ ensures that the altermagnetic contribution to the polarization rotation becomes sizable. A full analysis of magneto-acoustic setups that can be used to probe the Hall viscosity of magnetically ordered states will be presented elsewhere [90].

In summary, we have established the anomalous Hall viscosity as a natural bulk geometric response of altermagnets. Our group-theory analysis enables one to distinguish between ferromagnets, conventional antiferromagnets, and

altermagnets through the Hall viscosity, which in turn can be measured via magneto-acoustic measurements that are similar to the conventional acoustic Faraday effect. Microscopically, we demonstrated that because the Hall viscosity is governed by the strain-space Berry curvature, it becomes highly sensitive to the underlying electronic structure, being strongly enhanced near SOC-gapped Dirac crossings, Lifshitz transitions, and other band-structure singularities.

These results highlight that the Hall viscosity probes not only symmetry breaking, but also the topological properties of altermagnets. Often, the latter are described in terms of the properties of the momentum-space Berry curvature, which in altermagnets has a multipolar structure. While the magnetic moment direction or strain can distort it to produce a net nonzero momentum-space Berry curvature, the resulting anomalous Hall conductivity can only be measured in metallic or weakly semiconducting materials. In contrast, the strain-space Berry curvature displays a monopole structure even in unstrained pure altermagnets, and the resulting phonon Hall viscosity can be measured also in insulators, which comprise the vast majority of altermagnetic material candidates.

Acknowledgments: We are grateful to P. Brouwer, W. J. Meese, D. J. Schultz, J. Sinova, S. Sorn, D. Valentinis, and J. Venderbos for helpful discussions. I.J. and J.S. were supported by the German Research Foundation TRR 288-422213477 ELASTO-Q-MAT, Project A07. R.A. acknowledges partial support from the Brazilian agencies CNPq through a postdoctoral fellowship (Proc. 201212/2025-0) and from FAPESP (Grant No. 2023/05765-7). R.M.F. acknowledges support from the Research Corporation for Science Advancement through the Cottrell SEED Award CS-SEED-2025-012 and a Mercator Fellowship from the German Research Foundation (DFG) through Grant No. TRR 288, 422213477 Elasto-Q-Mat.

-
- [1] L. Šmejkal, J. Sinova, and T. Jungwirth, Beyond conventional ferromagnetism and antiferromagnetism: A phase with nonrelativistic spin and crystal rotation symmetry, *Phys. Rev. X* **12**, 031042 (2022).
 - [2] L. Šmejkal, J. Sinova, and T. Jungwirth, Emerging Research Landscape of Altermagnetism, *Phys. Rev. X* **12**, 040501 (2022).
 - [3] T. Jungwirth, R. M. Fernandes, E. Fradkin, A. H. MacDonald, J. Sinova, and L. Šmejkal, Altermagnetism: An unconventional spin-ordered phase of matter, *Newton* **1**, 100162 (2025).
 - [4] T. Jungwirth, J. Sinova, R. M. Fernandes, Q. Liu, H. Watanabe, S. Murakami, S. Nakatsuji, and L. Šmejkal, Symmetry, microscopy and spectroscopy signatures of altermagnetism, *Nature* **649**, 837 (2026).
 - [5] Y. Fang, J. Cano, and S. A. A. Ghorashi, Quantum Geometry Induced Nonlinear Transport in Altermagnets, *Phys. Rev. Lett.* **133**, 106701 (2024).
 - [6] D. S. Antonenko, R. M. Fernandes, and J. W. F. Venderbos, Mirror chern bands and weyl nodal loops in altermagnets, *Phys. Rev. Lett.* **134**, 096703 (2025).
 - [7] M. Roig, A. Kreisel, Y. Yu, B. M. Andersen, and D. F. Agterberg, Minimal models for altermagnetism, *Phys. Rev. B* **110**, 144412

- (2024).
- [8] P. Rao, A. Mook, and J. Knolle, Tunable band topology and optical conductivity in altermagnets, *Phys. Rev. B* **110**, 024425 (2024).
- [9] K. Parshukov, R. Wiedmann, and A. P. Schnyder, Topological responses from gapped Weyl points in 2D altermagnets, [arXiv:2403.09520](https://arxiv.org/abs/2403.09520) (2024).
- [10] T. Farajollahpour, R. Ganesh, and K. Samokhin, Light-induced charge and spin Hall currents in materials with C_4K symmetry, *npj Quantum Materials* **10**, 29 (2025).
- [11] K. Takahashi, C. R. W. Steward, M. Ogata, R. M. Fernandes, and J. Schmalian, Elasto-Hall conductivity and the anomalous Hall effect in altermagnets, *Phys. Rev. B* **111**, 184408 (2025).
- [12] N. Nagaosa, J. Sinova, S. Onoda, A. H. MacDonald, and N. P. Ong, Anomalous Hall effect, *Rev. Mod. Phys.* **82**, 1539 (2010).
- [13] L. Šmejkal, A. H. MacDonald, J. Sinova, S. Nakatsuji, and T. Jungwirth, Anomalous hall antiferromagnets, *Nature Reviews Materials* **7**, 482 (2022).
- [14] L. Šmejkal, R. González-Hernández, T. Jungwirth, and J. Sinova, Crystal time-reversal symmetry breaking and spontaneous hall effect in collinear antiferromagnets, *Science Advances* **6**, eaaz8809 (2020), <https://www.science.org/doi/pdf/10.1126/sciadv.aaz8809>.
- [15] K. P. Kluczyk, K. Gas, M. J. Grzybowski, P. Skupiński, M. A. Borysiewicz, T. Fas, J. Suffczyński, J. Z. Domagala, K. Grasza, A. Mycielski, M. Baj, K. H. Ahn, Vyborny, M. Sawicki, and M. Gryglas-Borysiewicz, Coexistence of anomalous Hall effect and weak magnetization in a nominally collinear antiferromagnet MnTe, *Phys. Rev. B* **110**, 155201 (2023).
- [16] L. Attias, A. Levchenko, and M. Khodas, Intrinsic anomalous Hall effect in altermagnets, *Phys. Rev. B* **110**, 094425 (2024).
- [17] M. Roig, Y. Yu, R. C. Ekman, A. Kreisel, B. M. Andersen, and D. F. Agterberg, Quasisymmetry-constrained spin ferromagnetism in altermagnets, *Phys. Rev. Lett.* **135**, 016703 (2025).
- [18] A. Osin, A. Levchenko, and M. Khodas, Extrinsic anomalous Hall effect in altermagnets, [arXiv:2511.03151](https://arxiv.org/abs/2511.03151) (2025).
- [19] Y. Guo, H. Liu, O. Janson, I. C. Fulga, J. van den Brink, and J. I. Facio, Spin-split collinear antiferromagnets: A large-scale ab-initio study, *Mater. Today Phys.* **32**, 100991 (2023).
- [20] J. Sødequist and T. Olsen, Two-dimensional altermagnets from high throughput computational screening: Symmetry requirements, chiral magnons, and spin-orbit effects, *Applied Physics Letters* **124** (2024).
- [21] X. Wan, S. Mandal, Y. Guo, and K. Haule, High-throughput search for metallic altermagnets by embedded dynamical mean field theory, *Phys. Rev. Lett.* **135**, 106501 (2025).
- [22] H.-Y. Ma, M. Hu, N. Li, J. Liu, W. Yao, J.-F. Jia, and J. Liu, Multifunctional antiferromagnetic materials with giant piezomagnetism and noncollinear spin current, *Nature communications* **12**, 2846 (2021).
- [23] S. Bhowal and N. A. Spaldin, Ferroically ordered magnetic octupoles in d -wave altermagnets, *Phys. Rev. X* **14**, 011019 (2024).
- [24] C. R. W. Steward, R. M. Fernandes, and J. Schmalian, Dynamic paramagnon-polarons in altermagnets, *Phys. Rev. B* **108**, 144418 (2023).
- [25] R. M. Fernandes, V. S. de Carvalho, T. Birol, and R. G. Pereira, Topological transition from nodal to nodeless Zeeman splitting in altermagnets, *Phys. Rev. B* **109**, 024404 (2024).
- [26] T. Aoyama and K. Ohgushi, Piezomagnetic properties in altermagnetic MnTe, *Phys. Rev. Mat.* **8**, L041402 (2024).
- [27] P. A. McClarty and J. G. Rau, Landau Theory of Altermagnetism, *Phys. Rev. Lett.* **132**, 176702 (2024).
- [28] K. V. Yershov, V. P. Kravchuk, M. Daghofer, and J. van den Brink, Fluctuation-induced piezomagnetism in local moment altermagnets, *Phys. Rev. B* **110**, 144421 (2024).
- [29] L. Attias, A. Levchenko, and M. Khodas, Intrinsic anomalous Hall effect in altermagnets, *Phys. Rev. B* **110**, 094425 (2024).
- [30] A. R. Chakraborty, J. Schmalian, and R. M. Fernandes, Magnetic-field-tuned randomness in inhomogeneous altermagnets, *Phys. Rev. B* **112**, 035146 (2025).
- [31] Y. Jiang, X. Zhang, H. Bai, Y. Tian, B. Zhang, W.-J. Gong, and X. Kong, Strain-engineering spin-valley locking effect in altermagnetic monolayer with multipiezo properties, *Applied Physics Letters* **126** (2025).
- [32] H. Schiff, P. McClarty, J. G. Rau, and J. Romhányi, Collinear altermagnets and their landau theories, *Phys. Rev. Res.* **7**, 033301 (2025).
- [33] M. Hu, X. Cheng, Z. Huang, and J. Liu, Catalog of C -paired spin-momentum locking in antiferromagnetic systems, *Phys. Rev. X* **15**, 021083 (2025).
- [34] B. Karetta, X. H. Verbeek, R. Jaeschke-Ubiergo, L. Šmejkal, and J. Sinova, Strain-controlled g - to d -wave transition in altermagnetic crsb, *Phys. Rev. B* **112**, 094454 (2025).
- [35] H. Radhakrishnan, B. Bell, C. Ortix, and J. Venderbos, Topological piezomagnetic effect in two-dimensional dirac quadrupole altermagnets, [arXiv:2602.05894](https://arxiv.org/abs/2602.05894) (2026).
- [36] M. Khodas, S. Mu, I. I. Mazin, and K. D. Belashchenko, Tuning of altermagnetism by strain, *Phys. Rev. B* **113**, 104422 (2026).
- [37] R. Ohlendorf, L. Buiarelli, H. M. Noad, A. P. Mackenzie, R. M. Fernandes, T. Birol, J. Schmalian, and E. Gati, Probing multipolar order in the candidate altermagnet MnF₂ through the elastocaloric effect under strain, [arXiv:2601.19343](https://arxiv.org/abs/2601.19343) (2026).
- [38] J. E. Avron, R. Seiler, and P. G. Zograf, Viscosity of quantum Hall fluids, *Phys. Rev. Lett.* **75**, 697 (1995).
- [39] M. Barkeshli, S. B. Chung, and X.-L. Qi, Dissipationless phonon Hall viscosity, *Phys. Rev. B* **85**, 245107 (2012).
- [40] B. Bradlyn, M. Goldstein, and N. Read, Kubo formulas for viscosity: Hall viscosity, Ward identities, and the relation with conductivity, *Phys. Rev. B* **86**, 245309 (2012).
- [41] T. Qin, J. Zhou, and J. Shi, Berry curvature and the phonon Hall effect, *Phys. Rev. B* **86**, 104305 (2012).
- [42] H. Shapourian, T. L. Hughes, and S. Ryu, Viscoelastic response of topological tight-binding models in two and three dimensions, *Phys. Rev. B* **92**, 165131 (2015).
- [43] T. Saito, K. Misaki, H. Ishizuka, and N. Nagaosa, Berry phase of phonons and thermal Hall effect in nonmagnetic insulators, *Phys. Rev. Lett.* **123**, 255901 (2019).
- [44] B. S. Kim, Modeling Hall viscosity in magnetic-skyrmion systems, *Phys. Rev. Res.* **2**, 013268 (2020).
- [45] M. Ye, L. Savary, and L. Balents, Phonon Hall viscosity in magnetic insulators, [arXiv:2103.04223](https://arxiv.org/abs/2103.04223) (2021).
- [46] Y. Zhang, Y. Teng, R. Samajdar, S. Sachdev, and M. S. Scheurer, Phonon Hall viscosity from phonon-spinon interactions, *Phys. Rev. B* **104**, 035103 (2021).
- [47] B. Flebus and A. H. MacDonald, Phonon Hall viscosity of ionic crystals, *Phys. Rev. Lett.* **131**, 236301 (2023).
- [48] H.-L. Kim, T. Saito, H. Yang, H. Ishizuka, M. J. Coak, J. H. Lee, H. Sim, Y. S. Oh, N. Nagaosa, and J.-G. Park, Thermal Hall effects due to topological spin fluctuations in YMnO₃, *Nature Communications* **15**, 243 (2024).
- [49] A. Shragai, E. Horsley, S. Kim, Y.-J. Kim, and B. Ramshaw, Phonon Hall viscosity and the intrinsic thermal Hall effect of α -RuCl₃, *Nature* **652**, 1166 (2026).

- [50] M. Müller, J. Schmalian, and L. Fritz, Graphene: A nearly perfect fluid, *Phys. Rev. Lett.* **103**, 025301 (2009).
- [51] J. M. Link, P. P. Orth, D. E. Sheehy, and J. Schmalian, Universal collisionless transport of graphene, *Phys. Rev. B* **93**, 235447 (2016).
- [52] A. A. Herasymchuk, E. V. Gorbar, and P. O. Sukhachov, Viscoelastic tensor and hydrodynamics of altermagnets, *Phys. Rev. B* **112**, 075150 (2025).
- [53] H. Jahn, Note on the Bhagavantam–Suranarayana method of enumerating the physical constants of crystals, *Acta Crystallographica* **2**, 30 (1949).
- [54] V stands, as usual, for a polar vector, square brackets imply a symmetric combination, curly brackets imply an anti-symmetric combination, and a denotes time reversal.
- [55] See Supplemental Material at <https://journals.aps.org/authors/supplemental-material-instructions> for details of tight binding model of the hexagonal system and acoustic Faraday effect.
- [56] B. Brekke, A. Brataas, and A. Sudbø, Two-dimensional altermagnets: Superconductivity in a minimal microscopic model, *Phys. Rev. B* **108**, 224421 (2023).
- [57] C.-C. Wei, X. Li, S. Hatt, X. Huai, J. Liu, B. Singh, K.-M. Kim, R. M. Fernandes, P. Cardon, L. Zhao, T. T. Tran, B. A. Frandsen, K. S. Burch, F. Liu, and H. Ji, $\text{La}_2\text{O}_3\text{Mn}_2\text{Se}_2$: A correlated insulating layered d-wave altermagnet, *Phys. Rev. Mater.* **9**, 024402 (2025).
- [58] P.-H. Chang, K. D. Belashchenko, and I. I. Mazin, Inverse lieb materials: Altermagnetism and more, *npj Quantum Materials* (2026).
- [59] L. Garcia-Gassull, A. Razpopov, P. P. Stavropoulos, I. I. Mazin, and R. Valentí, Microscopic origin of the magnetic interactions and their experimental signatures in altermagnetic $\text{La}_2\text{O}_3\text{Mn}_2\text{Se}_2$, *npj Spintronics* **4**, 9 (2026).
- [60] F. Zhang, X. Cheng, Z. Yin, C. Liu, L. Deng, Y. Qiao, Z. Shi, S. Zhang, J. Lin, Z. Liu, et al., Crystal-symmetry-paired spin–valley locking in a layered room-temperature metallic altermagnet candidate, *Nature Physics* **21**, 760 (2025).
- [61] B. Jiang, M. Hu, J. Bai, Z. Song, C. Mu, G. Qu, W. Li, W. Zhu, H. Pi, Z. Wei, et al., A metallic room-temperature d-wave altermagnet, *Nature Physics* **21**, 754 (2025).
- [62] B. Thapa, P.-H. Chang, K. Belashchenko, and I. I. Mazin, Is altermagnetism in vanadium oxychalcogenides a lost cause?, [arXiv:2602.18672](https://arxiv.org/abs/2602.18672) (2026).
- [63] Y.-K. Wang, S. Li, and S. A. Yang, Two-dimensional altermagnetic iron oxyhalides: Real chern topology and valley–spin–lattice coupling, *Nano Letters* **26**, 831 (2026).
- [64] B. Bell and J. Venderbos, Orbital piezomagnetic polarizability of pure insulating altermagnets, [arXiv:2602.10076](https://arxiv.org/abs/2602.10076) (2026).
- [65] I. Mazin, R. González-Hernández, and L. Šmejkal, Induced Monolayer Altermagnetism in $\text{MnP}(\text{S},\text{Se})_3$ and FeSe , [arXiv:2309.02355](https://arxiv.org/abs/2309.02355) (2023).
- [66] M. A. Vozmediano, M. Katsnelson, and F. Guinea, Gauge fields in graphene, *Physics Reports* **496**, 109 (2010).
- [67] N. Levy, S. A. Burke, K. Meaker, M. Panlasigui, A. Zettl, F. Guinea, A. C. Neto, and M. F. Crommie, Strain-induced pseudo–magnetic fields greater than 300 tesla in graphene nanobubbles, *Science* **329**, 544 (2010).
- [68] F. von Oppen, F. Guinea, and E. Mariani, Synthetic electric fields and phonon damping in carbon nanotubes and graphene, *Phys. Rev. B* **80**, 075420 (2009).
- [69] A. Cortijo, Y. Ferreirós, K. Landsteiner, and M. A. H. Vozmediano, Elastic gauge fields in weyl semimetals, *Phys. Rev. Lett.* **115**, 177202 (2015).
- [70] A. Cortijo, Y. Ferreirós, K. Landsteiner, and M. A. Vozmediano, Visco elasticity in 2d materials, *2D Materials* **3**, 011002 (2016).
- [71] Y. Ferreiros and M. A. H. Vozmediano, Elastic gauge fields and Hall viscosity of dirac magnons, *Phys. Rev. B* **97**, 054404 (2018).
- [72] Notice that whenever the chemical potential lies within the gap of the Dirac spectrum, the Hall viscosity is independent of both the order parameter ϕ and the spin-orbit coupling λ . However, the limit $\phi \rightarrow 0$ cannot be taken, since well-separated Dirac points exist only for sufficiently large values of the order parameter.
- [73] J. Ding, Z. Jiang, X. Chen, Z. Tao, Z. Liu, T. Li, J. Liu, J. Sun, J. Cheng, J. Liu, Y. Yang, R. Zhang, L. Deng, W. Jing, Y. Huang, Y. Shi, M. Ye, S. Qiao, Y. Wang, Y. Guo, D. Feng, and D. Shen, Large band splitting in g -wave altermagnet CrSb , *Phys. Rev. Lett.* **133**, 206401 (2024).
- [74] G. Yang, Z. Li, S. Yang, J. Li, H. Zheng, W. Zhu, Z. Pan, Y. Xu, S. Cao, W. Zhao, A. Jana, J. Zhang, M. Ye, Y. Song, L.-H. Hu, L. Yang, J. Fujii, I. Vobornik, M. Shi, H. Yuan, Y. Zhang, Y. Xu, and Y. Liu, Three-dimensional mapping and electronic origin of large altermagnetic splitting near Fermi level in CrSb , [arXiv:2405.12575](https://arxiv.org/abs/2405.12575) (2024).
- [75] C. Li, M. Hu, Z. Li, Y. Wang, W. Chen, B. Thiagarajan, M. Leandersson, C. Polley, T. Kim, H. Liu, C. Fulga, M. G. Vergniory, O. Janson, O. Tjernberg, and J. van den Brink, Topological Weyl Altermagnetism in CrSb , [arXiv:2405.14777](https://arxiv.org/abs/2405.14777) (2024).
- [76] M. Long, T. I. Weinberger, Z. Wu, M. F. Hansen, R. Tao, M. Shrestha, D. Graf, Y. Skourski, F. M. Grosche, and A. G. Eaton, 3d bulk-resolved g -wave magnetic order parameter symmetry in the metallic altermagnet CrSb , [arXiv:2601.14526](https://arxiv.org/abs/2601.14526) (2026).
- [77] I. Mazin, Altermagnetism in MnTe : Origin, predicted manifestations, and routes to detwinning, *Phys. Rev. B* **107**, L100418 (2023).
- [78] J. Krempaský, L. Šmejkal, S. W. D’Souza, M. Hajlaoui, G. Springholz, K. Uhlířová, F. Alarab, P. C. Constantinou, V. Strocov, D. Usanov, W. R. Pudlko, R. González-Hernández, A. Birk Hellenes, Z. Jansa, H. Reichlová, Z. Šobáň, R. D. Gonzalez Betancourt, P. Wadley, J. Sinova, D. Kriegner, J. Minár, J. H. Dil, and T. Jungwirth, Altermagnetic lifting of kramers spin degeneracy, *Nature* **626**, 517 (2024).
- [79] O. Amin, A. Dal Din, E. Golias, Y. Niu, A. Zakharov, S. Fromage, C. Fields, S. Heywood, R. Cousins, F. Maccherozzi, et al., Nanoscale imaging and control of altermagnetism in MnTe , *Nature* **636**, 348 (2024).
- [80] T. Osumi, S. Souma, T. Aoyama, K. Yamauchi, A. Honma, K. Nakayama, T. Takahashi, K. Ohgushi, and T. Sato, Observation of a giant band splitting in altermagnetic mnte, *Phys. Rev. B* **109**, 115102 (2024).
- [81] A. D. Din, D. Usanov, L. Šmejkal, S. D’Souza, F. Guo, O. Amin, E. Dawa, R. Champion, K. Edmonds, B. Kiraly, et al., Unconventional relativistic spin polarization of electronic bands in an altermagnet, [arXiv:2511.01690](https://arxiv.org/abs/2511.01690) (2025).
- [82] R. B. Regmi, H. Bhandari, B. Thapa, Y. Hao, N. Sharma, J. McKenzie, X. Chen, A. Nayak, M. El Gazzah, B. G. Márkus, et al., Altermagnetism in the layered intercalated transition metal dichalcogenide CoNb_4Se_8 , *Nature Communications* **16**, 4399 (2025).
- [83] J. Graham, T. Hicken, R. Regmi, M. Janoschek, I. Mazin, H. Luetkens, N. Ghimire, and Z. Guguchia, Local probe evidence supporting altermagnetism in $\text{Co}_{1/4}\text{NbSe}_2$, [arXiv:2503.09193](https://arxiv.org/abs/2503.09193) (2025).
- [84] N. Dale, O. A. Ashour, M. Vila, R. B. Regmi, J. Fox, C. W. Johnson, A. Fedorov, A. Stibor, N. J. Ghimire, and S. M. Griffin,

Non-relativistic spin splitting above and below the fermi level in a g -wave altermagnet, [arXiv:2411.18761 \(2024\)](#).

- [85] E. Day-Roberts, H. Wu, O. Erten, and A. Botana, An altermagnetic materials library in intercalated transition-metal dichalcogenides, [arXiv:2601.02481 \(2026\)](#).
- [86] C. Kittel, Interaction of spin waves and ultrasonic waves in ferromagnetic crystals, *Phys. Rev.* **110**, 836 (1958).
- [87] S. Wang and J. Crow, Acoustic Faraday rotation, *IEEE Transactions on Magnetics* **7**, 138 (1971).
- [88] Y. Lee, T. M. Haard, W. P. Halperin, and J. A. Sauls, Discovery of the acoustic Faraday effect in superfluid $^3\text{He-B}$, *Nature* **400**, 431 (1999).
- [89] A. Sytcheva, U. Löw, S. Yasin, J. Wosnitzer, S. Zherlitsyn, P. Thalmeier, T. Goto, P. Wyder, and B. Lüthi, Acoustic Faraday

effect in $\text{Tb}_3\text{Ga}_5\text{O}_{12}$, *Phys. Rev. B* **81**, 214415 (2010).

- [90] R. Aquino, I. Jang, J. Schmalian, and R. M. Fernandes, Probing the Hall viscosity of altermagnets using a modified acoustic Faraday effect, unpublished.
- [91] H. T. Stokes, D. M. Hatch, and B. J. Campbell, *ISOTROPY Software Suite*, [iso.byu.edu](#) (2022).
- [92] M. I. Aroyo, J. M. Perez-Mato, C. Capillas, E. Kroumova, S. Ivantchev, G. Madariaga, A. Kirov, and H. Wondratschek, Bilbao Crystallographic Server: I. Databases and crystallographic computing programs, *Zeitschrift für Kristallographie-Crystalline Materials* **221**, 15 (2006).

END MATTER

In Table I we list the independent non-vanishing elements of the Hall viscosity tensor η_{ijkl}^H generated by different types of ferromagnetic and altermagnetic order in the most symmetric tetragonal, hexagonal, and cubic point groups [25]. The presence of SOC is assumed. We used the software Isotropy [91] and the Bilbao Crystallographic Server [92] to obtain these results. Note that additional elements follow from the relations $\eta_{ijkl}^H = \eta_{jikl}^H = \eta_{ijlk}^H = -\eta_{klij}^H$.

We consider separately the altermagnetic (AM) and ferromagnetic (FM) order parameters. When the order parameter is multi-dimensional, we show explicitly the order parameter components that are non-zero, e.g. $(1, 0, 0)$ or $(\sqrt{3}, 1)$. In this table, the (x, y, z) coordinates refer to the coordinates in the magnetically ordered state, which can be rotated with respect to the coordinates of the paramagnetic phase depending on which order parameter components condense [92]. Note that, for the cubic point group, the i -wave AM order parameter that transforms as the A_{1g}^- irrep does not have a non-zero Hall viscosity tensor element.

Point Group	AM irrep.	Hall viscosity tensor	FM irrep.	Hall viscosity tensor
tet. D_{4h} ($4/mmm$)	A_{1g}^- (g -wave)	$\eta_{xxzz}^H = \eta_{yyzz}^H$	A_{2g}^-	$\eta_{xxxy}^H = -\eta_{yyxy}^H, \eta_{xzyz}^H$
	B_{1g}^- (d -wave)	$\eta_{xxzz}^H = -\eta_{yyzz}^H, \eta_{xxxy}^H$	E_g^- (1, 0)	$\eta_{xxxy}^H, \eta_{yyxy}^H, \eta_{xzyz}^H, \eta_{xyzz}^H$
	B_{2g}^- (d -wave)	$\eta_{xxxy}^H = \eta_{yyxy}^H, \eta_{xyzz}^H$	E_g^- (1, 1)	$\eta_{xxyz}^H, \eta_{yyyz}^H, \eta_{zzyz}^H, \eta_{xyxz}^H$
hex. D_{6h} ($6/mmm$)	A_{1g}^- (i -wave)	$\eta_{xxzz}^H = \eta_{yyzz}^H$	A_{2g}^-	$\eta_{xxxy}^H = -\eta_{yyxy}^H, \eta_{xzyz}^H$
	B_{1g}^- (g -wave)	$\eta_{xxzz}^H = -\eta_{yyzz}^H = -\eta_{xyyz}^H$	E_{1g}^- (1, 0)	$\eta_{xxyz}^H, \eta_{yyyz}^H, \eta_{zzyz}^H, \eta_{xyxz}^H$
	B_{2g}^- (g -wave)	$\eta_{xxyz}^H = -\eta_{yyyz}^H = \eta_{xyxz}^H$	E_{1g}^- ($\sqrt{3}, 1$)	$\eta_{xxyz}^H, \eta_{yyyz}^H, \eta_{zzyz}^H, \eta_{xyxz}^H$
	E_{2g}^- (1, 0) (d -wave)	$\eta_{xxyy}^H, \eta_{xxzz}^H, \eta_{yyzz}^H$		
	E_{2g}^- ($\sqrt{3}, 1$)	$\eta_{xxxy}^H, \eta_{yyxy}^H, \eta_{zzxy}^H, \eta_{xzyz}^H$		
cub. O_h ($m\bar{3}m$)	A_{2g}^- (d -wave)	$\eta_{xxxy}^H = \eta_{yyzz}^H = \eta_{zzxx}^H$	T_{1g}^- (1, 0, 0)	$\eta_{xxxy}^H = -\eta_{yyxy}^H, \eta_{xzyz}^H$
	E_g^- (1, 0) (d -wave)	$\eta_{xxzz}^H = \eta_{yyzz}^H$	T_{1g}^- (1, 1, 1)	$\eta_{xxxy}^H = -\eta_{yyxy}^H, \eta_{xzyz}^H,$ $\eta_{xxzz}^H = -\eta_{yyzz}^H = \eta_{yzxy}^H$
	E_g^- ($\sqrt{3}, 1$)	$\eta_{xxzz}^H = -\eta_{yyzz}^H, \eta_{xxxy}^H$		
	T_{2g}^- (1, 0, 0) (d -wave)	$\eta_{xxxy}^H = \eta_{yyxy}^H, \eta_{xyzz}^H$		
	T_{2g}^- (1, 1, 1)	$\eta_{xxzz}^H = \eta_{yyzz}^H, \eta_{xyxz}^H = \eta_{xxyx}^H = -\eta_{yyyz}^H$		

TABLE I. Non-zero elements of the Hall viscosity tensor η_{ijkl}^H in point groups D_{4h} , D_{6h} , and O_h for altermagnetic (AM) and ferromagnetic (FM) orders.

Supplementary Material: Anomalous Hall viscosity of altermagnets

Iksu Jang,¹ Rui Aquino,^{2,3,4} Jörg Schmalian,^{1,5} and Rafael M. Fernandes^{2,3}

¹*Institute for Theory of Condensed Matter, Karlsruhe Institute of Technology, Karlsruhe 76131, Germany*

²*Department of Physics, The Grainger College of Engineering,*

University of Illinois Urbana-Champaign, Urbana, Illinois 61801, USA

³*Anthony J. Leggett Institute for Condensed Matter Theory, The Grainger College of Engineering,*
University of Illinois Urbana-Champaign, Urbana, Illinois 61801, USA

⁴*ICTP South American Institute for Fundamental Research, São Paulo, SP, Brazil*

⁵*Institute for Quantum Materials and Technologies,*

Karlsruhe Institute of Technology, Karlsruhe 76131, Germany

(Dated: June 26, 2026)

CONTENTS

S1. Hall viscosity beyond the adiabatic approximation:	1
S2. Tetragonal d -wave altermagnetic model	2
A. Numerical values of TB parameters	2
B. Dirac theory and emergent gauge fields	2
S3. Hexagonal g -wave altermagnetic model	3
A. Symmetries of CrSb	3
B. Tight-binding parameters	5
S4. Hall viscosity and k_z -dependent Lifshitz transitions	6
A. Details of the Berry curvature calculation	6
References	6

S1. HALL VISCOSITY BEYOND THE ADIABATIC APPROXIMATION:

In the main text we used the adiabatic approximation to determine the Hall viscosity, an approach that is well defined for gapped systems, but may be problematic in the presence of gapless excitations. To address this issue we rederive Eq. (5) without relying on the adiabatic approximation. We consider the following strain-dependent action

$$S[\Psi^\dagger, \Psi, \varepsilon] = \int_{\tau, \mathbf{k}} \left[\Psi_{\mathbf{k}}^\dagger(\tau) \partial_\tau \Psi_{\mathbf{k}}(\tau) + \Psi_{\mathbf{k}}^\dagger(\tau) \mathcal{H}_{0, \mathbf{k}} \Psi_{\mathbf{k}}(\tau) + \varepsilon_{\alpha\beta}(\tau) \Psi_{\mathbf{k}}^\dagger(\tau) \mathcal{H}_{\varepsilon, \mathbf{k}}^{\alpha\beta} \Psi_{\mathbf{k}}(\tau) \right]. \quad (\text{S1})$$

By integrating out the fermion fields, we obtain the effective action in terms of the strain field ε .

$$S_{\text{eff}} = \frac{1}{2} \sum_{i\Omega} \varepsilon_{\alpha\beta}(i\Omega) \varepsilon_{\gamma\delta}(-i\Omega) \Pi^{\alpha\beta, \gamma\delta}(i\Omega),$$

$$\Pi^{\alpha\beta, \gamma\delta}(i\Omega) = T \sum_{\mathbf{k}, i\omega} \text{tr} \left[\mathcal{H}_{\varepsilon, \mathbf{k}}^{\alpha\beta} G_{\mathbf{k}, i\omega} \mathcal{H}_{\varepsilon, \mathbf{k}}^{\gamma\delta} G_{\mathbf{k}, i\omega+i\Omega} \right], \quad (\text{S2})$$

where $G_{\mathbf{k}, i\omega} = [i\omega - \mathcal{H}_{0, \mathbf{k}}]^{-1}$. Performing the Matsubara sum and the analytic continuation $i\Omega \rightarrow \omega + i\eta$, we obtain

$$\Pi^{\alpha\beta, \gamma\delta}(\omega) = \sum_{\mathbf{k}, n \neq m} n_F(\xi_{\mathbf{k}n}) \left[\frac{\langle u_{\mathbf{k}, m} | \mathcal{H}_{\varepsilon, \mathbf{k}}^{\alpha\beta} | u_{\mathbf{k}, n} \rangle \langle u_{\mathbf{k}, n} | \mathcal{H}_{\varepsilon, \mathbf{k}}^{\gamma\delta} | u_{\mathbf{k}, m} \rangle}{\xi_{\mathbf{k}n} - \xi_{\mathbf{k}m} + \omega + i\eta} - (n \leftrightarrow m) \right]. \quad (\text{S3})$$

Here, $|u_{\mathbf{k}, n}\rangle$ and $\xi_{\mathbf{k}n}$ are the n -th eigenvector and eigenvalue of $\mathcal{H}_{0, \mathbf{k}}$, respectively. This serves as finite ω contribution to the elastic tensor. To first order in ω , we obtain

$$S_{\text{eff}} = -\frac{1}{2} \int \frac{d\omega}{2\pi} i\omega \varepsilon_{\alpha\beta}(\omega) \varepsilon_{\gamma\delta}(-\omega) \eta^{\alpha\beta, \gamma\delta} \quad (\text{S4})$$

from which we readily identify the Hall viscosity

$$\eta^{\alpha\beta,\gamma\delta} = \sum_{\mathbf{k}} \sum_{n \neq m} \frac{2n_F(\xi_{\mathbf{k}n})}{(\xi_{\mathbf{k}m} - \xi_{\mathbf{k}n})^2} \text{Im} \left[\langle u_{\mathbf{k},m} | \mathcal{H}_{\epsilon,\mathbf{k}}^{\alpha\beta} | u_{\mathbf{k},n} \rangle \langle u_{\mathbf{k},n} | \mathcal{H}_{\epsilon,\mathbf{k}}^{\gamma\delta} | u_{\mathbf{k},m} \rangle \right] \quad (\text{S5})$$

in agreement with Eqs. (2) and (5).

S2. TETRAGONAL d -WAVE ALTERMAGNETIC MODEL

A. Numerical values of TB parameters

For the results presented in Fig. 2 in the main text, we used the following numerical values of parameters

$$t_2 = t_1/2, \quad t_d = 2t_1, \quad \lambda = 2t_1, \quad J = t_1, \quad \phi = \phi_c/2 \quad (\text{S6})$$

$$g_1^{(A_1)} = g_1^{(B_2)} = \alpha t_1, \quad g_3^{(A_1)} = \alpha t_d, \quad g_0^{(A_1)} = \alpha t_2 \quad (\text{S7})$$

with $t_1 = 1$ and $\alpha = 8$.

For Fig. 3 in main text, comparing results obtained from the Dirac theory and the tight binding model, we use following numerical values of parameters:

$$t_2 = 0, \quad t_d = 0.705t_1, \quad \lambda = 0.025t_1, \quad J = t_1/2, \quad \phi = \phi_c/2, \quad (\text{S8})$$

which gives $v_1 = v_3 = 1.41t_1$, $m = 0.175t_1$, with

$$g_1^{(A_1)} = g_1^{(B_2)} = \alpha t_1, \quad g_3^{(A_1)} = \alpha t_d, \quad g_0^{(A_1)} = 0, \quad (\text{S9})$$

where $\alpha = 8$.

B. Dirac theory and emergent gauge fields

Here, we expand the Lieb-lattice Hamiltonian Eqs. (7) and (8) in the vicinity of the Dirac points. In the absence of spin orbit coupling, i.e. for $\lambda = 0$, there are four Dirac nodes at the boundary of the Brillouin zone. To make the analysis easier, we consider the Brillouin zone defined by $k_x, k_y \in (0, 2\pi)$ as shown in Fig. 3(a). Let us assume without restriction that $t_d, J, \phi > 0$. Provided $0 < \phi < \phi_c = 4t_d/J$, spin up states have two Dirac points located at (k_0, π) and $(2\pi - k_0, \pi)$, while spin down states have Dirac points at (π, k_0) and $(\pi, 2\pi - k_0)$, as depicted in Fig. 3(a), with the momentum scale $k_0 = \arccos(2\phi/\phi_c - 1)$. For $J = 0$ ($\phi_c = \infty$), $k_0 = \pi$ and the Dirac points merge at $(\pm\pi, \pm\pi)$ to become quadratic band touching points. In the vicinity of these Dirac points and for small spin-orbit coupling, we obtain

$$\mathcal{H}_0^{\uparrow,\kappa}(\mathbf{p}) = \kappa v_1 p_y \tau_1 + \kappa v_3 p_x \tau_3 + m \tau_2, \quad (\text{S10})$$

where $\kappa = \pm 1$ stands for the valley indices ($\kappa = +1$: (k_0, π) , $\kappa = -1$: $(2\pi - k_0, \pi)$) and \mathbf{p} is a momentum vector measured with respect to each valley momentum. The velocities are given as $v_1 = 2t_1 \sqrt{\phi/\phi_c}$ and $v_3 = 4t_d \sqrt{\phi/\phi_c} \sqrt{1 - \phi/\phi_c}$, while $m = \lambda \sqrt{1 - \phi/\phi_c}$ is the mass. For the down spins we have

$$\mathcal{H}_0^{\downarrow,\kappa}(\mathbf{p}) = \kappa v_1 p_x \tau_1 - \kappa v_3 p_y \tau_3 - m \tau_2, \quad (\text{S11})$$

where $\kappa = \pm 1$ stands for the valley points (π, k_0) and $(\pi, 2\pi - k_0)$ respectively.

The strain terms at the Dirac points are

$$\begin{aligned} \mathcal{H}_\epsilon^{\sigma,\kappa} &= 2 \left(\varepsilon_{xx} + \varepsilon_{yy} \right) (\bar{g}_0 \tau_0 + \sigma \bar{g}_3 \tau_3) - 4 \varepsilon_{xy} \bar{g}_1 \tau_1 \\ &+ 2 \left(\varepsilon_{xx} - \varepsilon_{yy} \right) \bar{g}'_3 \tau_3 \end{aligned} \quad (\text{S12})$$

with $\bar{g}_0 = 2g_0^{(A_{1g})}(\phi/\phi_c - 1)$, $\bar{g}_3 = 2g_3^{(A_{1g})}\phi/\phi_c$, $\bar{g}'_3 = 2g^{(B_{1g})}(\phi/\phi_c - 1)$, and $\bar{g}_1 = g^{(B_{2g})}\sqrt{1 - \phi/\phi_c}$. The spin dependence of the strain term is a consequence of the fact that the location of the Dirac points is different for spin-up

and spin-down states. This yields the stress tensors $T_{xx+yy}^\sigma = 2(\bar{g}_0\tau_0 + \sigma\bar{g}_3\tau_3)$, $T_{xx-yy} = 2\bar{g}_3\tau_3$, and $T_{xy} = -4\bar{g}_1\tau_1$. The Hamiltonian in the presence of strain is then given by Eq. (10) in the main text, with gauge fields

$$\begin{aligned}\mathcal{A}^{\uparrow,\kappa} &= 2\kappa \left(\frac{\bar{g}'_3(\varepsilon_{xx} - \varepsilon_{yy}) - \bar{g}_3(\varepsilon_{xx} + \varepsilon_{yy})}{v_3}, \frac{2\bar{g}_1\varepsilon_{xy}}{v_1} \right) \\ \mathcal{A}^{\downarrow,\kappa} &= 2\kappa \left(\frac{2\bar{g}_1\varepsilon_{xy}}{v_1}, \frac{\bar{g}'_3(\varepsilon_{xx} - \varepsilon_{yy}) + \bar{g}_3(\varepsilon_{xx} + \varepsilon_{yy})}{v_3} \right)\end{aligned}\quad (\text{S13})$$

and Dirac matrices $\alpha^\uparrow = (\tau_3, \tau_1)$, $\alpha^\downarrow = (\tau_1, \tau_3)$, and $\beta = \tau_2$, obeying the usual Clifford algebra. For the velocities, it holds $v^{\uparrow,\kappa} = \kappa(v_3, v_1)$ while $v^{\downarrow,\kappa} = \kappa(v_1, -v_3)$. By analyzing the Hall conductivity of a single gapped Dirac point with respect to these emergent gauge fields, we obtain the result given in the main text. Using Eq. (S13) and Eq. (13), we then obtain the following effective action in terms of the strain field:

$$S_{\text{eff}} = \frac{8g_1g_3}{t_1t_d}\sigma_{xy}^H \int_{t,x} (\varepsilon_{xx} + \varepsilon_{yy})\dot{\varepsilon}_{xy} \quad (\text{S14})$$

which gives $\eta_{xx+yy,xy}^H = \frac{8g_1g_3}{t_1t_d}\sigma_{xy}^H$.

S3. HEXAGONAL g -WAVE ALTERMAGNETIC MODEL

In this section, we provide a detailed description of the hexagonal model for g -wave altermagnetism corresponding to space group $P6_3/mmc$ (No. 194), which is relevant for CrSb, following Ref. [1].

A. Symmetries of CrSb

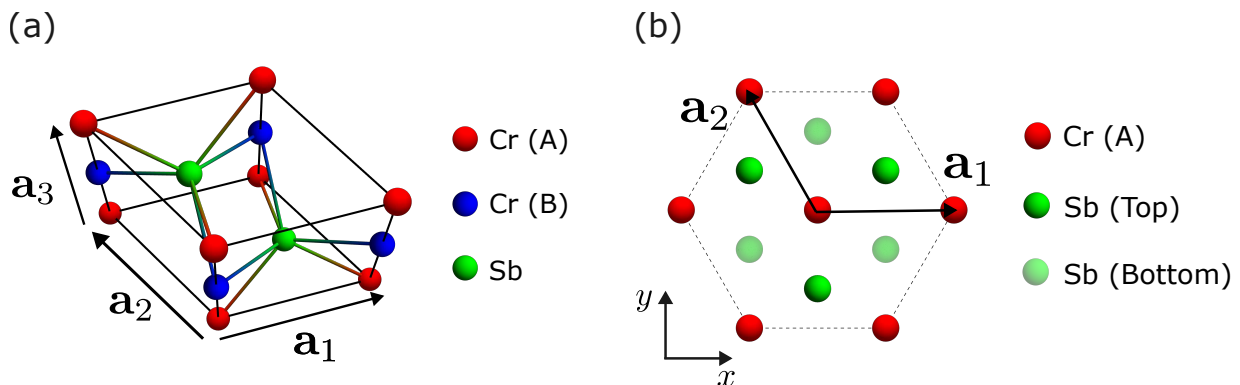


FIG. S1: (a) Unit-cell of the CrSb. (b) Top-view of the CrSb lattice.

Fig. S1 illustrates the unit cell of CrSb, which crystallizes in space group 194 ($P6_3/mmc$), as well as the top-view of the lattice. We define the lattice vectors \mathbf{a}_1 , \mathbf{a}_2 , and \mathbf{a}_3 according to the coordinates in Fig. S1 to construct the space group representations.

The generators of the space group, expressed in Seitz notation $\{R|\mathbf{t}\}$, are:

$$\mathbb{1}, \quad \{3_{001}|0, 0, 0\}, \quad \{2_{001}|0, 0, 1/2\}, \quad \{2_{110}|0, 0, 0\}, \quad \mathcal{I}$$

where the indices nml for the rotation axes and translation vectors denote the direction $n\mathbf{a}_1 + m\mathbf{a}_2 + l\mathbf{a}_3$. Following Ref. [1], we consider the electrons on the two Cr sublattices (A, B) as the primary degrees of freedom. Sublattices A and B are located at $(0, 0, 0)$ and $(0, 0, 1/2)$, respectively.

The field operators in momentum space are given by:

$$c_{\alpha,\sigma}(\mathbf{k}) = \frac{1}{\sqrt{N}} \sum_{\mathbf{R}} e^{-i\mathbf{k}\cdot(\mathbf{R}+\bar{\eta}_\alpha)} c_{\alpha,\sigma}(\mathbf{R}), \quad (\text{S15})$$

with sublattice vectors $\vec{\eta}_A = 0$ and $\vec{\eta}_B = \frac{1}{2}\mathbf{a}_3$. We thus define the four-component spinor as:

$$\psi(\mathbf{k}) = (c_{A,\uparrow}(\mathbf{k}) \ c_{A,\downarrow}(\mathbf{k}) \ c_{B,\uparrow}(\mathbf{k}) \ c_{B,\downarrow}(\mathbf{k}))^T. \quad (\text{S16})$$

Generator	Operator Transformation	Vector Relation
$\{3_{001} 0, 0, 0\}$	$\begin{cases} c_A^\dagger(\mathbf{R}) \rightarrow c_A^\dagger(\mathbf{R}') \\ c_B^\dagger(\mathbf{R}) \rightarrow c_B^\dagger(\mathbf{R}') \end{cases}$	$\mathbf{R}' = 3_{001}\mathbf{R}, \begin{cases} 3_{001}\mathbf{a}_1 = \mathbf{a}_2 \\ 3_{001}\mathbf{a}_2 = -\mathbf{a}_1 - \mathbf{a}_2 \end{cases}$
$\{2_{001} 0, 0, 1/2\}$	$\begin{cases} c_A^\dagger(\mathbf{R}) \rightarrow c_B^\dagger(\mathbf{R}') \\ c_B^\dagger(\mathbf{R}) \rightarrow c_A^\dagger(\mathbf{R}' + \mathbf{a}_3) \end{cases}$	$\mathbf{R}' = 2_{001}\mathbf{R}, \begin{cases} 2_{001}\mathbf{a}_1 = -\mathbf{a}_1 \\ 2_{001}\mathbf{a}_2 = -\mathbf{a}_2 \end{cases}$
$\{2_{110} 0, 0, 0\}$	$\begin{cases} c_A^\dagger(\mathbf{R}) \rightarrow c_A^\dagger(\mathbf{R}') \\ c_B^\dagger(\mathbf{R}) \rightarrow c_B^\dagger(\mathbf{R}' - \mathbf{a}_3) \end{cases}$	$\mathbf{R}' = 2_{110}\mathbf{R}, \begin{cases} 2_{110}\mathbf{a}_1 = \mathbf{a}_2 \\ 2_{110}\mathbf{a}_2 = \mathbf{a}_1 \\ 2_{110}\mathbf{a}_3 = -\mathbf{a}_3 \end{cases}$
\mathcal{I}	$\begin{cases} c_A^\dagger(\mathbf{R}) \rightarrow c_A^\dagger(\mathbf{R}') \\ c_B^\dagger(\mathbf{R}) \rightarrow c_B^\dagger(\mathbf{R}' - \mathbf{a}_3) \end{cases}$	$\mathbf{R}' = -\mathbf{R}$

TABLE S1: Space-group symmetry operations on the fermionic operators for space group 194, relevant to hexagonal CrSb.

Space group operations (194)	Point group operations (D_{6h})
$\{6_{001} 0, 0, 1/2\} = \{2_{001} 0, 0, 1/2\}\{3_{001} 0, 0, 0\}$	C_6
$\{3_{001} 0, 0, 0\}$	C_3
$\{2_{001} 0, 0, 1/2\}$	C_2
$\{2_{100} 0, 0, 0\}, \{2_{110} 0, 0, 0\}, \{2_{010} 0, 0, 0\}$	$C_2'' (2_{100})$
$\{2_{110} 0, 0, 0\}, \{2_{210} 0, 0, 0\}, \{2_{120} 0, 0, 0\}$	$C_2' (2_{120})$
\mathcal{I}	\mathcal{I}

TABLE S2: Correspondence between the symmetry operations in the space group 194 and the symmetry operations of the point group D_{6h} .

Table S1 summarizes the action of the symmetry operations of the space group on the fermion operators. In the spinor representation, these operations are:

$$\{3_{001}|0, 0, 0\}\psi(\mathbf{k})\{3_{001}|0, 0, 0\}^{-1} = (\tau_0 \otimes e^{i\frac{\pi}{3}\sigma_z})\psi(3_{001}\mathbf{k}), \quad (\text{S17})$$

$$\{2_{001}|0, 0, 1/2\}\psi(\mathbf{k})\{2_{001}|0, 0, 1/2\}^{-1} = e^{i\frac{k_z}{2}}(\tau_x \otimes e^{i\frac{\pi}{2}\sigma_z})\psi(2_{001}\mathbf{k}), \quad (\text{S18})$$

$$\{2_{110}|0, 0, 0\}\psi(\mathbf{k})\{2_{110}|0, 0, 0\}^{-1} = (\tau_0 \otimes e^{i\frac{\pi}{2}\sigma_x})\psi(2_{110}\mathbf{k}), \quad (\text{S19})$$

$$\mathcal{I}\psi(\mathbf{k})\mathcal{I}^{-1} = (\tau_0 \otimes \sigma_0)\psi(-\mathbf{k}). \quad (\text{S20})$$

It is convenient to use the correspondence between operations in space group 194 and those of the underlying D_{6h} point group, as shown in Table S2. This correspondence is obtained by comparing the character table of each case. Using this correspondence, the fermionic bilinears can be classified into irreducible representations of D_{6h} as follows:

- $\psi^\dagger(\mathbf{k})\tau_0\psi(\mathbf{k}) : A_{1g}$
- $\psi^\dagger(\mathbf{k})\tau_1\psi(\mathbf{k}) : A_{1g}$
- $\psi^\dagger(\mathbf{k})\tau_2\psi(\mathbf{k}) : B_{2g}^-$
- $\psi^\dagger(\mathbf{k})\tau_3\psi(\mathbf{k}) : B_{2g}$

where the minus superscript indicates a time-reversal odd irrep.

B. Tight-binding parameters

Using the spinors introduced above, it is now straightforward to construct the Hamiltonian $H = \sum_{\mathbf{k}} \psi^\dagger(\mathbf{k}) \mathcal{H}_{\mathbf{k}} \psi(\mathbf{k})$. Following Ref. [1], the strain-free part of the Hamiltonian $\mathcal{H}_{\mathbf{k},0}$ is given by:

$$\mathcal{H}_{\mathbf{k},0} = \varepsilon_{0,\mathbf{k}} + t_{1,\mathbf{k}}\tau_1 + t_{3,\mathbf{k}}\tau_3 + \tau_2 \vec{\lambda}_{\mathbf{k}} \cdot \vec{\sigma} + J\phi\tau_3\sigma_3, \quad (\text{S21})$$

where the hopping terms are:

$$\varepsilon_{0,\mathbf{k}} = t_1 \left(\cos k_x + 2 \cos \frac{k_x}{2} \cos \frac{\sqrt{3}k_y}{2} \right) + t_2 \cos k_z - \mu, \quad (\text{S22})$$

$$t_{1,\mathbf{k}} = t_3 \cos \frac{k_z}{2}, \quad t_{3,\mathbf{k}} = t_4 \sin k_z f_y (f_y^2 - 3f_x^2), \quad (\text{S23})$$

$$\lambda_{x,\mathbf{k}} = \lambda \cos \frac{k_z}{2} (f_x^2 - f_y^2), \quad \lambda_{y,\mathbf{k}} = -2\lambda \cos \frac{k_z}{2} f_x f_y, \quad \lambda_{z,\mathbf{k}} = \lambda_z \sin \frac{k_z}{2} f_x (f_x^2 - 3f_y^2), \quad (\text{S24})$$

and with hexagonal form factors defined as $f_x = \sin k_x + \sin \frac{k_x}{2} \cos \frac{\sqrt{3}k_y}{2}$ and $f_y = \sqrt{3} \cos \frac{k_x}{2} \sin \frac{\sqrt{3}k_y}{2}$. Here, x is the direction parallel to the \mathbf{a}_1 in Fig. S1, corresponding to the crystallographic direction [100]. Note that the antiferromagnetic order parameter ϕ transforms as $B_{1g}^- = B_{2g} \otimes A_{2g}^-$, since $\psi^\dagger(\mathbf{k})\tau_3\psi(\mathbf{k})$ transforms as B_{2g} , as reflected in the transformation properties of the function $t_{3,\mathbf{k}}$, and σ_3 transforms as A_{2g}^- .

The strain Hamiltonian $\mathcal{H}_{\mathbf{k},\varepsilon}$ consists of two parts corresponding to the shear components that transform as the E_{1g} (out-of-plane shear) and E_{2g} (in-plane shear) irreps of the point group D_{6h} :

$$\mathcal{H}_{\mathbf{k},\varepsilon} = \mathcal{H}_{\mathbf{k},\varepsilon}^{(E_{1g})} + \mathcal{H}_{\mathbf{k},\varepsilon}^{(E_{2g})}, \quad (\text{S25})$$

$$\mathcal{H}_{\mathbf{k},\varepsilon}^{(E_{1g})} = g_{\tau_1}^{(E_{1g})} \left[\varepsilon_{xz} f_{1,\mathbf{k}}^{(xz)} + \varepsilon_{yz} f_{1,\mathbf{k}}^{(yz)} \right] \tau_1 + g_{\tau_3}^{(E_{1g})} \left[\varepsilon_{xz} f_{3,\mathbf{k}}^{(xz)} + \varepsilon_{yz} f_{3,\mathbf{k}}^{(yz)} \right] \tau_3, \quad (\text{S26})$$

$$\begin{aligned} \mathcal{H}_{\mathbf{k},\varepsilon}^{(E_{2g})} = & g_{\tau_1}^{(E_{2g})} \left[(\varepsilon_{xx} - \varepsilon_{yy}) f_{1,\mathbf{k}}^{(x^2-y^2)} - 2\varepsilon_{xy} f_{1,\mathbf{k}}^{(xy)} \right] \tau_1 \\ & + g_{\tau_3}^{(E_{2g})} \left[(\varepsilon_{xx} - \varepsilon_{yy}) f_{3,\mathbf{k}}^{(x^2-y^2)} - 2\varepsilon_{xy} f_{3,\mathbf{k}}^{(xy)} \right] \tau_3 \\ & + g_{\text{SOC}}^{(E_{2g})} f_{\text{SOC},\mathbf{k}} [(\varepsilon_{xx} - \varepsilon_{yy}) \sigma_x - 2\varepsilon_{xy} \sigma_y] \tau_2 \end{aligned} \quad (\text{S27})$$

where $g_i^{(\Gamma)}$ are the coupling constants and the form factors $f_{i,\mathbf{k}}^{(\alpha)}$ are:

$$f_{1,\mathbf{k}}^{(xz)} = -\frac{8}{\sqrt{3}} \sin \frac{k_z}{2} \sin \frac{k_x}{2} \left(2 \cos \frac{k_x}{2} + \cos \frac{\sqrt{3}k_y}{2} \right), \quad f_{3,\mathbf{k}}^{(xz)} = -4 \sin \frac{k_x}{2} \sin \frac{\sqrt{3}k_y}{2}, \quad (\text{S28})$$

$$f_{1,\mathbf{k}}^{(yz)} = -8 \sin \frac{k_z}{2} \cos \frac{k_x}{2} \sin \frac{\sqrt{3}k_y}{2}, \quad f_{3,\mathbf{k}}^{(yz)} = \frac{4}{\sqrt{3}} \left(\cos k_x - \cos \frac{k_x}{2} \cos \frac{\sqrt{3}k_y}{2} \right), \quad (\text{S29})$$

$$f_{1,\mathbf{k}}^{(x^2-y^2)} = \frac{8}{\sqrt{3}} \cos \frac{k_z}{2} \left(\cos k_x - \cos \frac{k_x}{2} \cos \frac{\sqrt{3}k_y}{2} \right), \quad f_{3,\mathbf{k}}^{(x^2-y^2)} = -\sqrt{3} \sin k_z \cos \frac{k_x}{2} \sin \frac{\sqrt{3}k_y}{2}, \quad (\text{S30})$$

$$f_{1,\mathbf{k}}^{(xy)} = 8 \cos \frac{k_z}{2} \sin \frac{k_x}{2} \sin \frac{\sqrt{3}k_y}{2}, \quad f_{3,\mathbf{k}}^{(xy)} = \sin k_z \left(\sin k_x + \sin \frac{k_x}{2} \cos \frac{\sqrt{3}k_y}{2} \right), \quad (\text{S31})$$

$$f_{\text{SOC},\mathbf{k}} = \cos \frac{k_z}{2}. \quad (\text{S32})$$

The results shown in the main text were obtained for the following set of tight-binding parameters:

$$\begin{aligned} t_2 = 0.6t_1, \quad t_3 = 0.3t_1, \quad t_4 = 0.2t_1, \quad \lambda = \lambda_z = 0.5t_1, \quad \phi_z = 0.5t_1, \\ g_{\tau_1}^{(E_{1g})} = g_{\tau_3}^{(E_{1g})} = g_{\tau_1}^{(E_{2g})} = g_{\tau_3}^{(E_{2g})} = g_{\text{SOC}}^{(E_{2g})} = 8t_1. \end{aligned}$$

For the quantitative analysis of the Hall viscosity it is necessary to relate the typical values of the electron-strain couplings $g = \alpha t_1$ to the hopping elements t_1 . Consider hopping elements between orbitals of angular momentum ℓ and ℓ' at a distance r and with equilibrium distance r_0 . They behave like $t(r) \sim t_0 (r/r_0)^{-(\ell+\ell'+1)} \approx t_0 \left(1 + \alpha \frac{r-r_0}{r_0} \right)$ [2, 3].

Then, the dimensionless constant is $\alpha = \ell + \ell' + 1$. Hence, $\alpha = 1$ describes hopping between two s -orbitals, while $\alpha = 5$ refers to hopping between two d -orbitals. If the hopping is a consequence of a second order process between two orbitals with angular momentum ℓ via an intermediate orbital with angular momentum ℓ' , we obtain $\alpha = 2(\ell + \ell' + 1)$. Hence hopping between two d -orbitals ($\ell = 2$) via a p -orbital ($\ell' = 1$) yield the value used here, $\alpha = 8$.

S4. HALL VISCOSITY AND k_z -DEPENDENT LIFSHITZ TRANSITIONS

We demonstrate that the abrupt changes in the Hall viscosity of the hexagonal g -wave altermagnet are directly linked to Lifshitz transitions. Figs. S2(a)–(c) show the changes in the Fermi surface as the chemical potential varies within the narrow range in which the Hall viscosity shows sharp changes. In all cases, we observe Lifshitz transitions from closed to open Fermi surfaces around the high-symmetry L and M points, establishing the connection between Lifshitz transitions and changes in the Hall viscosity. In contrast, when the Lifshitz transition takes place near the H and K points, the Hall viscosity does not display sharp changes, as shown in Fig. S2(d). This distinction arises because the strain-dependent Hamiltonian $\mathcal{H}_{e,\mathbf{k}}$ at these points either vanishes or couples to only a single component of the strain tensor, thereby precluding a Hall response.

A. Details of the Berry curvature calculation

In the numerical calculation of the Hall viscosity, in order to avoid high symmetry points that usually coincide with time-reversal invariant-momenta, we set our grids as follows:

$$\mathbf{k}_{ijk} = \mathbf{G}_1 \frac{i-0.5}{N_1} + \mathbf{G}_2 \frac{j-0.5}{N_2} + \mathbf{G}_3 \frac{k-0.5}{N_3}, \quad \begin{cases} i = 1, \dots, N_1 \\ j = 1, \dots, N_2 \\ k = 1, \dots, N_3 \end{cases} \quad (\text{S33})$$

where \mathbf{G}_1 , \mathbf{G}_2 , and \mathbf{G}_3 are the reciprocal lattice vectors defined as:

$$\mathbf{G}_1 = 2\pi \left(\hat{x} + \frac{1}{\sqrt{3}} \hat{y} \right), \quad \mathbf{G}_2 = \frac{4\pi}{\sqrt{3}} \hat{y}, \quad \mathbf{G}_3 = 2\pi \hat{z}. \quad (\text{S34})$$

We found that the numerical calculation of the Hall viscosity tensor for the hexagonal g -wave model converges poorly as a function of grid size. This is because of the change of the projected two-dimensional Fermi surface topology as a function of k_z . Near the k_z planes associated with these Lifshitz transitions, the k_x, k_y -integrated Berry curvature, defined as $\bar{\Omega}(k_z) \equiv \int_{k_x, k_y} \Omega(k_x, k_y, k_z)$, exhibits severe oscillations depending on the grid resolution. Consequently, the Hall viscosity, which is proportional to $\int_{k_z} \bar{\Omega}(k_z)$, converges extremely slowly, failing to stabilize even when the grid dimensions $N_1 \times N_2 \times N_3$ approach $500 \times 500 \times 500$.

To resolve this issue, we introduced the Fermi-Dirac distribution function with temperature scales $T \approx \frac{8t_1}{N_1 N_2 N_3}$. This thermal broadening acts as a numerical low-pass filter that effectively smooths out the topological transitions across the discrete grid slices. As a result, the Hall viscosity tensor converges significantly faster and remains robust against variations in grid configuration. For the numerical results presented in the main text, we set $N_1 = N_2 = N_3 = 240$, which corresponds to a regularizing temperature scale of $T/t_1 = 5.8 \times 10^{-7}$.

We note that, although the numerical grid was chosen to avoid all high-symmetry points, certain momentum points still exhibit large local Berry curvature values. This high concentration makes it difficult to clearly identify the underlying symmetry properties of the Berry curvature. To resolve this, we introduce a regularized Berry curvature for Figs. 4(d) and 4(e) in main text, defined as:

$$\Omega_{\alpha\beta\gamma\delta}^{(l),\text{reg}}(\mathbf{k}) = 2\text{Im} \sum_{m \neq l} \frac{\gamma_{ml}^{\alpha\beta}(\mathbf{k})^* \gamma_{ml}^{\gamma\delta}(\mathbf{k})}{(\xi_{\mathbf{k}l} - \xi_{\mathbf{k}m})^2 + \delta^2}. \quad (\text{S35})$$

For these figures, we set $\delta = 0.5t_1$. Note that this regularized version is strictly used for visual presentation in these specific plots; all calculations for the Hall viscosity tensor presented in the main text were performed using the exact formulation with $\delta = 0$.

[1] M. Roig, A. Kreisel, Y. Yu, B. M. Andersen, and D. F. Agterberg, Minimal models for altermagnetism, Phys. Rev. B **110**, 144412 (2024).

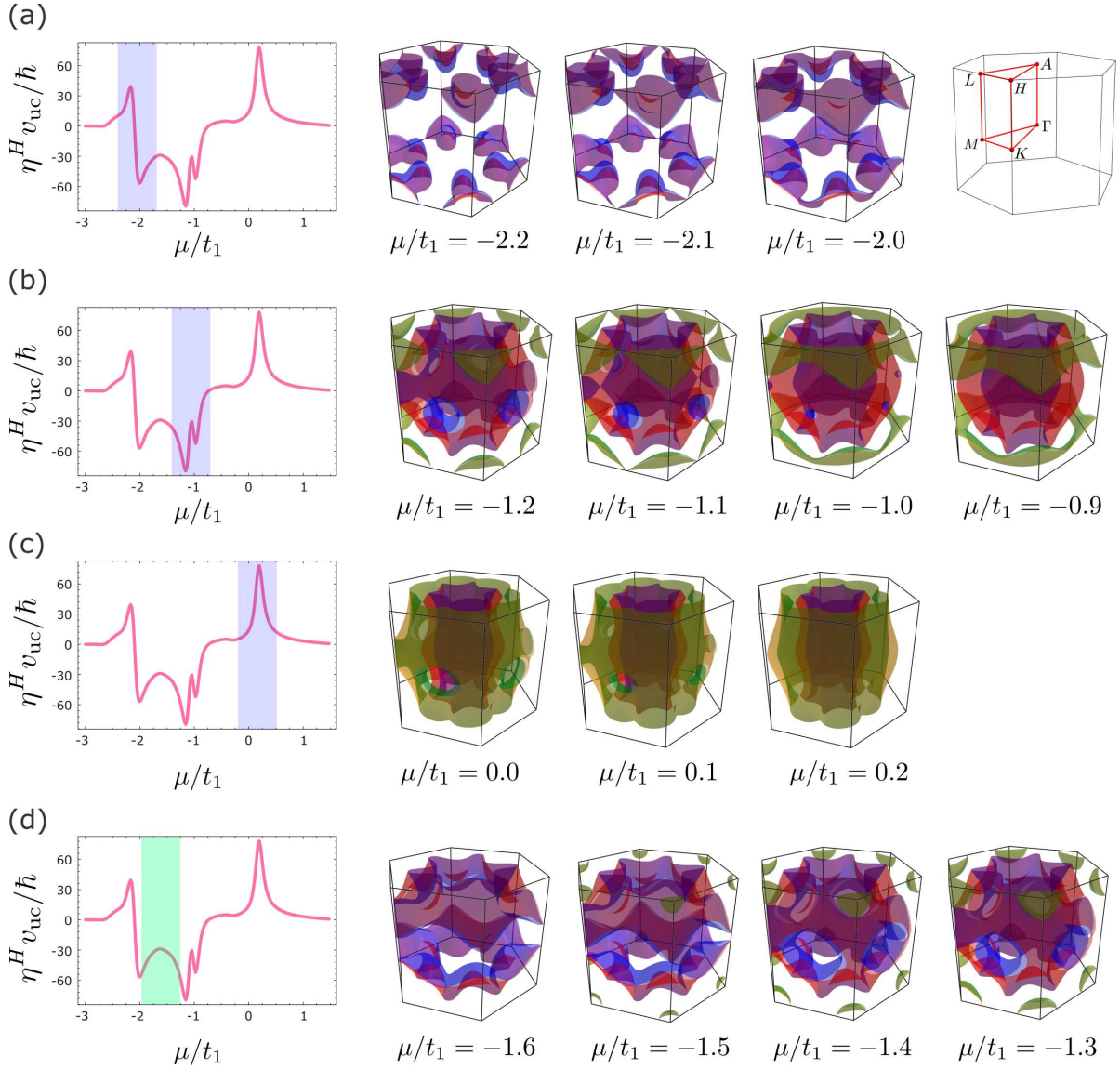


FIG. S2: Hall viscosity and Lifshitz transitions in the hexagonal g -wave altermagnetic model. (a)–(c) Hall viscosity within the chemical potential intervals (a) $-2.3 \lesssim \mu/W \lesssim -1.9$, (b) $-1.3 \lesssim \mu/W \lesssim -0.8$, and (c) $-0.1 \lesssim \mu/W \lesssim 0.3$ (blue-shaded regions), accompanied by the evolution of the Fermi surface. These panels demonstrate that Lifshitz transitions at the L and M high-symmetry points correlate with abrupt changes in the Hall viscosity. (d) In contrast, Lifshitz transitions at the H and K points within the range $-1.7 \lesssim \mu/W \lesssim -1.2$ (green-shaded region) do not exhibit a similar behavior.

- [2] W. A. Harrison, *Electronic structure and the properties of solids: the physics of the chemical bond*, Courier Corporation (2012).
- [3] K. Takahashi, C. R. W. Steward, M. Ogata, R. M. Fernandes, and J. Schmalian, *Elasto-Hall conductivity and the anomalous Hall effect in altermagnets*, *Phys. Rev. B* **111**, 184408 (2025).